Biomedical Signal Processing and Control 88 (2024) 105321

Contents lists available at ScienceDirect

Biomedical Signal Processing and Control

journal homepage: www.elsevier.com/locate/bspc

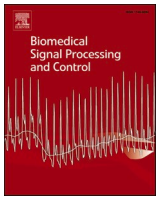

Towards a precision medicine Solution for optimal pediatric Laparoscopy: An exploratory data analysis for features Selections

Lorenzo Carnevale [a,*], Giuseppe Floramo [c], Donatella Di Fabrizio [b], Salvatore Arena [b], Angela Simona Montalto [b], Pietro Impellizzeri [b], Carmelo Romeo [b], Massimo Villari [a]

[a] Department of Mathematics and Computer Science, Physics and Hearth Sciences, University of Messina, Messina, Italy
[b] Department of Human Pathology of Adults and Developmental Age "Gaetano Barresi", Messina, Italy
[c] Paediatric Surgery, University of Brescia, Brescia, Italy

ARTICLE INFO

Keywords:
Precision Surgery
Abdominal Compliance
Descriptive Analysis
VarianceThreshold
Pearson Correlation
Shapiro-Wilk Test

ABSTRACT

Over the past years, healthcare methodologies were commonly applied to all patients affected by the same pathology as an overall treatment. However, recent scientific works were mainly aimed at personalized care, according to the patient's clinical conditions and morphological characteristics. Pediatric surgery was also involved in this process, although laparoscopy has been set aside so far. In this regard, the physical characteristic that correlates intra-abdominal pressure and intra-abdominal volume (i.e., abdominal com-pliance) was always studied as a unique curve. This work aims to propose an alternative approach to treat laparoscopy surgery and abdominal compli-ance for pediatric individuals, which is based on personalized medicine. We perform an exploratory data analysis considering a real dataset, in order to study the data model (i.e., descriptive univariate and multivariate analysis) and the predictors (i.e., variance thresholding, Shapiro-Wilk test, Pearson's correlation coefficient) that will allow physicians to build clusters of pediatric individuals. Data analysis proves that there are strong correlations among features referring to thorax circumference and xifo-bisialic lenght with the sum of thorax and pelvis volumes. This leads to identify the optimal number of clusters through the Elbow method.

1. Introduction

In healthcare, a concept of medicine tailored to individual differences is emerging [1], which considers genetic variability, the environment, the characteristics of the microbiome, and the lifestyle of individual people. The meticulous process of identifying therapies and cures in such a subjective way is called precision medicine. In other words, it refers to a new approach to medicine that is based on the individual features of the patient rather than using a classic one-size-fits-all approach. Therefore, physicians move from treatments aimed at the average patient to tailor-made therapies for the individual who has specific characteristics to obtain better results thanks, for example, to targeted prevention strategies and the use of ad-hoc drugs. Such innovation is made possible by the great variety of physiological parameters evidenced nowadays by modern technologies, i.e., artificial intelligence (AI) and big data. (Fig. 1.).

In this regard, pediatric surgery represents a new frontier where precision medicine solutions can help personalize one or more operation phases. For example, in laparoscopic surgery, an increase in intra-abdominal pressure is induced by the insufflation of $CO2$ in order to expand the abdominal cavity and create a working space to explore it. However, an excessive insufflation can result in Intra-Abdominal Hypertension (IAH), a condition that causes i) diaphragmatic compression, ii) decrease in pulmonary compliance, iii) de-crease in venous return, iv) reduction of cardiac output, v) hypercapnia, vi) hypoxia, and an increase in sympathetic cardiac activity with hyper-activation of the renin-angiotensin-aldosterone system [2,3]. Traditionally, IAH is defined as an Intra-Abdominal Pressure (IAP) higher than 12 mmHg but, during laparoscopy, it is often necessary to make IAP higher than this value to obtain an optimal working space. Although international guidelines [3] recommend working with the lowest IAP value that ensures an adequate working space, the standard practice is to initially set the IAP value without further adjustments regardless of the amount of generated Intra–Abdominal Volume (IAV).

* Corresponding author.
E-mail addresses: lcarnevale@unime.it (L. Carnevale), g.floramo@unibs.it (G. Floramo), donatella.difabrizio@studenti.unime.it (D.D. Fabrizio), arena.salvatore@unime.it (S. Arena), angelasimona.montalto@unime.it (A.S. Montalto), pietro.impellizzeri@unime.it (P. Impellizzeri), romeoc@unime.it (C. Romeo), mvillari@unime.it (M. Villari).

https://doi.org/10.1016/j.bspc.2023.105321
Received 15 April 2023; Received in revised form 9 July 2023; Accepted 31 July 2023
Available online 17 October 2023

Previous methodologies [4] related to traditional medicine focus on ana-lyzing the Pressure-Volume (P-V) curve with the scope of determining ab-dominal wall compliance, that is the limits of IAP and the volume of gas re-quired to obtain the maximal intraperitoneal space for laparoscopic surgery. Instead, a novel approach based on AI aims to determine clusters of pedi-atric individuals, where a multi-parametric system identifies an ideal range of IAP values based on their morphological characteristics. This turns into a dedicated P-V curve associated with a cluster of patients, and therefore, into a safe range within which the physicians can determine the amount of $CO2$ to insufflate for avoiding the IAH.

To our knowledge, this is the first investigation on a dataset collected during a laparoscopy surgery. Therefore, before starting with a predictive model design, in this paper, we provide an exploratory data analysis, studying the data model and the predictors that will allow clinical operators to forecast the best treatment with the purpose of personalizing the patient's therapy. Therefore, we determine the best features that minimizes the number of clusters and will lay the foundation for building a set of P-V curves. Trying to have a summary of all of that, the main scientific contributions of this research are:

- definition of a data acquisition protocol of laparoscopy instrumentation for studying the P-V curve of pediatric patients;
- in-depth exploratory data analysis of pediatric individuals to study the best predictors for making clusters of P-V curve;
- feature selection to minimize the number of clusters.

The rest of the paper is organized as follows. Section 2 describes related works and compares our proposal with the scientific literature. A brief overview of the instrumentation, the protocol designed to acquire data be-fore, during, and after laparoscopy, along with a characterization of all fea-tures are discussed in Section 3. Results are reported in Section 4, including the exploratory data analysis and feature selection. A discussion about the results is, instead, available in Section 5, i.e., how exploiting results for opti-mizing the number of clusters. Finally, conclusions and future directions are summarized in Section 6.

2. Related works

From the time precision medicine was announced as a research initiative that aims to accelerate progress toward a new era of healthcare [1], several works have been proposed by the scientific community. Even though most of the time precision medicine was applied to study cancer diseases [5,6,7], fur-ther applications have been investigated, such as the classification of skeletal muscles using ultrasound imaging [8] and the application of transformer to medical image segmentation [9]. Also, the application of precision medicine to surgery is not new [10,11,12]. For example, in minimally invasive opera-tions, the use of robot automation can enhance precision [13], whereas aug-mented reality offers further opportunities for precision in surgery [14]. AI was successfully applied to both dermatology [15] and endoscopy [16] in preci-sion surgery. In this regard, numerous trials on either open or robot-assisted radical cystectomy [17] revealed no significant differences in progression-free and overall survival thanks to perioperative and intraoperative parameters. In the same way, data collected during routine presurgical evaluations pushed scientists to propose a machine learning methodology [18] to achieve preci-sion epilepsy surgery. AI algorithms could also enhance the value of mass spectrometry imaging [19,20], as well as predict cancer development and, therefore, dictate the ideal timing for surgery [21]. Trying to sum up all of that, precision medicine in surgery is expected to specialize in treatment and master multiple technologies.

For all we know, no scientific results have been published about practical studies or applications of precision medicine in laparoscopy surgery. This work is, therefore, the first of its kind. Laparoscopy is, more specifically, a minimally invasive surgical technique used for diagnostic purposes, which al-lows the study of the abdominal cavity and pelvic excavation. In this surgery, there is a direct relationship between pressure and volume, which is charac-terized by the abdominal compliance [22,23,24]. For example, comparing abdominal cavity with a hydraulic system, Keulenaer et al. show in [25] how abdominal pressure is between 3 mmHg and 7 mmHg. Therefore, according to the World Society on Abdominal Compartment Syndrome (WSACS1) consensus definitions, abdominal compliance [26,27,28] is defined as a measure of the ease of abdominal expansion, which is determined by the elasticity of the abdominal wall and diaphragm [29]. It should be expressed as the change in IAV per change in IAP (mL [mm Hg] −1).

The study of abdominal compliance and, therefore, the relationship be-tween abdominal ΔP and ΔV is influenced by different morphological pa-rameters [30], such as age, size, BMI, bowel content, body wall thickness, organomegaly, space occupying lesions, position of the patient, and type of ventilation, etc. It is a sigmoid-shaped relationship [31] that forms a different curve for each patient according to different parameters. However, what is nowadays proposed is studying a single P-V curve for all patients by means of the methodologies described as follows. Zhou et al. [31] studied the elas-ticity values of the abdominal wall in children of different ages. The results show that the abdomen expands by an average of 17 % in response to the pneumoperitoneum and the abdominal pressure–volume relationship follows a sigmoid pattern. Mulier et al. [22] show how three points of the P-V curve can be sufficient to calculate the relationship between pressure and volume of the abdominal cavity. The gain in volume is, indeed, obtained only up to

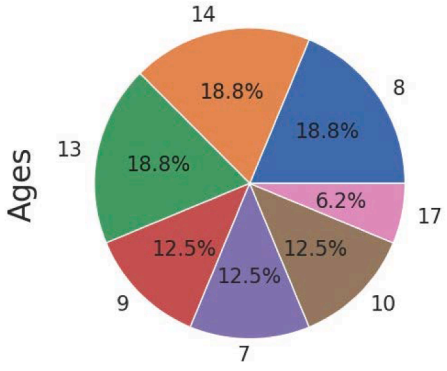

(a) Amount of ages values

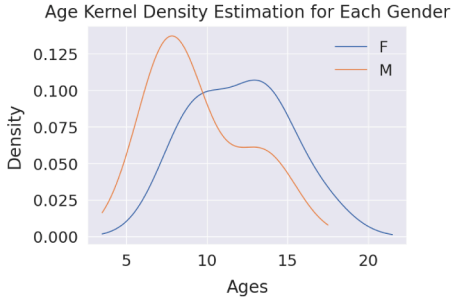

(b) Multivariate KDE relationship between gender and ages.

Fig. 1. Study of the samples balance by ages.

certain levels of pressure depending on biomechanical properties, i.e., on the morpho-structural characteristics of the patient. Authors, pointed out how higher pressure does not always generate steadily higher volumes. Neverthe-less, this study used a simple linear function, while it has been demonstrated that the P-V curve has a sigmoid-shaped [31]. Vlot et al. [24] studied the P-V curve on pigs with weight of approximately 30 kg, very close to the weight of a pediatric individual. They analyzed gains of volume through im-ages of computed tomography executed during the laparoscopic surgery at a regular period of time. Furthermore, authors also analyzed how abdominal diameters change at different pneumoperitoneum pressure. Becker et al. [32] describe the correlation between the fat/muscle wall ratio, the percentage of wall fat, the muscle thickness, and the thickness of the fat. As a result, they highlighted how abdominal compliance is influenced by several variables, mainly by the thickness of the abdominal wall fat. The mathematical model adopted in this work is based on the Young's module. Unfortunately, the study is however carried on a cohort of adult patients and not pediatric individuals.

To summarize, several studies have been carried on the relationship be-tween pressure and volume for determining the abdominal compliance, which is a key value on the laparoscopy surgery. Many of them, indeed, pointed out how morphological attributes of patients contribute to characterize the research of the inflection point of the P-V sigmoid. However, no one had the insight of proposing a personalized study. What we describe in the follow-.

ing is just a prior approach for extracting the right morphological attributes that will help us in creating a cluster of P-V curves tailored on the pediatric individuals.

3. Material and methods

In the following, we report the materials used to achieve the goals above-mentioned and the methodology applied in the hospital to acquire data from patients during a surgery. In this regard, the laparoscope instrumentation was used to collect part of dataset, which features are later summarized. The use and collection of these materials (e.g., instrumentation and dataset) was approved by the ethic committee and regulated by the data acquisition methodology. The proposed methodology is therefore tailored to the need of the Pediatric Surgery Unit of Polyclinic G. Martino in Messina, guaranteeing the safety of patient while performing an innovative research.

3.1. Instrumentation

Laparoscopy is a minimally invasive surgical technique that involves the use of dedicated equipment with the aim of giving access to both the ab-dominal and pelvic cavity, avoiding large incisions. It is a method that can have both diagnostic and therapeutic intent. Access to the abdominal cavity is achieved by placing a trocar through the umbilical scar (in most cases a 10 mm Hasson trocar) into which the scope is inserted. The Hasson trocar allows the gases' insufflation. As a consequence, IAP increases and creates a laparoscopy working space. If necessary, it is possible to insert another trocar to use the surgical instruments.

The laparoscope is a rigid metal tube, it is a two-channels device (a fiber optic system and a lighting system). Thanks to this, images can be projected in real time. The laparoscope's lenses are organized according to the Hopkins system (a series of cylindrical lenses separated by air chambers where the refraction of light takes place); the camera lens can be angled from 0° to 30°. The camera head is attached to the end of the scope and contains the imager. The role of the imager is to convert the optical image into an electrical signal. The insufflator is a device that regulate the insufflation of the gas used ($CO2$) and control the IAP in order to guarantee its maintenance. The operator can set from the instrument panel pressure to reach (0–30 mmHg) and the gas emission flow (0–30 L/min).

3.2. Data acquisition protocol

Data were collected by the Pediatric Surgery Unit of Polyclinic G. Mar-tino in Messina (Italy). Our dataset is currently based on 16 patients aged between 7 and 18 years. Data were collected between May 2022 and June 2022. Patients did not have complicated pathologies (i.e, peritonitis, skele-tal or structural deformities). Patients' sensitive data were anonymized to respect the European General Data Protection Regulation (GDPR). For ex-ample, patients' names were replaced with the string *patient-#*, where the symbol # represents the sample's number.

The data acquisition process started in the operating room before the surgical approach and intraoperative while using the standard laparoscopic instrumentation. Raw data were manually reported in a Microsoft Excel sheet and preprocessed as follows. The volumes of the abdominal compart-ment were computed when evaluated at different values of insufflated IAP. Volumes were obtained by approximating the abdomen and pelvis respec-tively to an elliptical cylinder and a spherical cap.

Measures were taken in the supine position at three different phases: i) basal, that is before the surgery, ii) after 50 % of insufflation pressure, and iii) after the maximum point of IAP reached during surgery time. The elliptical cylinder volume was computed as described in the equation (1):

$$V = \pi^* a^* b^* h \tag{1}$$

where $a = A - P$ length, b is the bis-spino-iliac line length, and h is the xipho-bisiliac length. The spherical cap volume was instead computed as described in the equation (2):

$$r = a2 + h2 \tag{2}$$

where h is the ration between midpoint bis-spino-iliac line and the pubic symphysis length and $a = bis - iliacline/2$. The total volume was computed by summing the results of the equations (1) and (2). By our convention, the measurements were made out of the right side of the abdominal wall.

The protocol of this study was submitted to the ethics committee and approved before being applied to patients.

3.3. Features characteristic

After the data acquisition process, the dataset contains 16 entries char-acterized by 49 attributes. All features collected per patient are summarized below.

Age, gender, height, weight represent four features related to the phys-ical characteristics of patients. The values of height and weight are, respectively, expressed in *cm* and *Kg*.

BMI represents the body mass index, a biometric datum expressed as the ratio between the weight and height square of an individual. This is typically used as an indicator of the state of ideal weight. The value is expressed in $Kg/cm2$.

IAP 0 %, 35 %, 50 %, 75 %, 100 % represent five features related to IAP at different insufflation rates. The IAP 0 % is always considered 0 by default, meaning that no CO2 is insufflated. The values are expressed in *mmHg*.

Thorax circumference represents a feature related to the circumference of the thorax meaning that no CO2 is insufflated, before the surgical approach. The value is expressed in *cm*.

Waist circumference 0 %, 50 %, 100 % represent three features related to the circumference of the waist at different insufflation rates. The waist circumference 0 % is the original measure of the patient, meaning that no CO2 is insufflated, waist circumference 50 % is the length at 50 % of IAP reached during the surgical approach, waist circumference 100 % is the length at a maximum of IAP reached during the surgical approach. The values are expressed in *cm*.

Hips circumference 0 %, 50 %, 100 % represent three features

related to the circumference of the hips at different insufflation rates. The hips circumference 0 % is the original measure of the patient, meaning that no CO2 is insufflated, hips circumference 50 % is the length at 50 % of IAP reached during the surgical approach, hips circumference 100 % is the length at a maximum of IAP reached during the surgical approach. The values are expressed in *cm*.

Antero-posterior diameter 0 %, 50 %, 100 % represent three features re-lated to anteroposterior abdomen diameter. The A-P 0 % is the diam-eter of the abdomen before surgical approach (meaning that no CO"is insufflated); the A-P 50 % is the diameter of the abdomen at 50 % of IAP; the A-P 100 % is the diameter of the abdomen at 100 % of IAP. The values are expressed in *cm*.

Jugular notch/xiphoid length 0 % represents one feature related to the length between the jugular notch and xiphoid (meaning that no *CO*2 is insufflated), before the surgical approach. The value is expressed in *cm*.

Xifo-Bisiliac length 0 %, 50 %, 100 % represent three features measured to a xiphoidal point at midpoint of bisiliac line before the surgical approach (meaning that no CO2 is insufflated), at 50 % of IAP reached during surgery and at 100 % of the IAP reached during surgery. The values are expressed in *cm*.

Midpoint bispinoiliac line/pubic symphysis length 0 %, 50 %, 100 % represent three features related to the length between the bispinoil-iac line's midpoint and pubic symphysis before surgical approach (0 %, meaning that no CO2 is insufflated), at 50 % of IAP reached during surgery (50 %) and at maximum point of IAP reached during surgery (100 %). The values are expressed in *cm*.

Bis-spino-iliac length 0 %, 50 %, 100 % represent three features related to the length between the left and right anterosuperior iliac spine at different insufflation rates. The bis-spino-iliace length 0 % is the original measure of the patient, meaning that no CO2 is insufflated, the bis-spino-iliac length 50 % is the length at 50 % of IAP reached during surgery and the bis-spino-iliac 100 % is the length reached maximum IAP reached during surgery. The values are expressed in *cm*.

Rectus of the abdomen m. (under the navel) thickness represents one feature obtained by a US study before surgery. It is the Rectus muscle's thickness in its lower portion (under the navel). The value is expressed in *cm*.

Rectus of the abdomen m. (over the navel) thickness represents one feature obtained by a USA study before surgery. It is the Rectus muscle's thickness in its upper portion (over the navel). The value is expressed in *cm*.

Oblique and Transverse m. (under the navel) thickness represents one feature obtained by a USA study before surgery. It is the Oblique and Transverse muscle's thickness in its lower portion (under the navel). The value is expressed in *cm*.

Oblique and Transverse m. (over the navel) thickness represents one feature obtained by a USA study before surgery. It is the Oblique and Transverse muscle's thickness in its upper portion (under the navel). The value is expressed in *cm*.

Lateral fat layer thickness represents one feature obtained by a USA study before surgery. It is an average value between lateral fat layer thickness under and over the navel. The value is expressed in *cm*.

Medial fat layer thickness represents one feature obtained by a USA study before surgery. It is an average value between medial fat layer thickness under and over the navel. The value is expressed in *cm*.

Lateral abdominal wall thickness represents one feature related to a USA value obtained before surgery by the sum of lateral fat layer thickness and average value between Oblique and Transverse m. thickness over and under the navel. The value is expressed in *cm*.

Medial abdominal wall thickness represents one feature related to a USA value obtained before surgery by sum of: medial fat layer thickness and average value between Rectus m. thickness over and under the navel.

Abdominal volume 0 %, 50 %, 100 % represent three features related to volume of abdomen at different insufflation rates. The abdominal vol-ume 0 % is the original measure of the patient, meaning that no *CO*2 is insufflated, the abdominal volume 50 % is the volume at 50 % of maxi-mum value of IAP reached, the abdominal volume 100 % is the volume at maximum IAP reached. The values are expressed in *cm*3.

Pelvic volume 0 %, 50 %, 100 % represent three features related to the volume of the pelvis at different insufflation rates. The pelvic volume 0 % is the original measure of the patient, meaning that no *CO*2 is insufflated, the pelvic volume 50 % is the volume at 50 % of the maximum value of IAP reached, the pelvic volume 100 % is the volume at maximum IAP reached. The values are expressed in *cm*3.

Volume 0 %, 35 %, 50 %, 75 %, 100 % represent five features related to to-tal volume at different insufflation rates. The volume 0 % is the original measure of the patient, meaning that no *CO*2 is insufflated the volume 50 % is the volume at 50 % of the maximum value of IAP reached, and the volume 100 % is the volume at maximum IAP reached. The values are expressed in *cm*3.

Finally, a descriptive statistics including those that summarize the cen-tral tendency, dispersion and shape of a dataset's distribution (i.e., mean, standard deviation, minimum, and maximum values) is shown in the Table 1..

4. Result

Characterization of the dataset is achieved with an exploratory data anal-ysis (EDA), a best practice for studying what data tell beyond the formal modeling or hypothesis testing task. We used a Jupyter Notebook with a virtualenv kernel Python 3.10.6 64-bit and various packages for visually ex-ploring the dataset. Matplotlib 3.6.1 and seaborn 0.12.0 were used to have attractive and informative statistical graphics, while data analysis was car-ried on using pandas 1.5.0 and scipy 1.9.2.

4.1. Descriptive analysis

The dataset does not have any missing value, and therefore no action was required to clean it. The number of male samples is 7, representing the 44 % of total samples, whereas the number of female samples is 9, representing the 56 % of total samples. The balance of dataset in terms of patient-ages is also respected, as shown in Fig. 2(a), generally covering the entire spectrum of pediatric patients over 7 years old. For selected features (i.e., ages, BMI) we also studied whether an observation is unlikely or very unlikely. Indeed, the probability density is the relationship between the outcomes of a ran-dom variable and its probability. If the random variable is continuous, the probability is computed with a probability density function (PDF), which shape represents the probability distribution. The latter is then helpful for determining if an observation might be an outlier or anomaly. Given that we do not know a priori the probability distribution of our features, we must estimate it through a probability density estimation. There are few meth-ods to estimate the probability density (i.e., histogram) but we used a non-parametric density estimation to potentially study not common distributions (i.e., bimodal distribution). The kernel density estimation (KDE) is then an algorithm used to approximate the probability distribution under these con-straints, which uses a mathematical function known as kernel that returns.

a probability for a given value of random variable with the intent to inter-polate the probabilities across the range of outcomes. The kernel function weights the contribution of observations from a data sample based on their relationship or distance to a given query sample for which the probability is requested. Formally, let ($x1$, $x2$, …, xn) be independent and identically dis-tributed samples drawn from some univariate distribution with an unknown density f at any given point $\times$, we are interested in estimating the shape and recognizing the pattern of the function f. Its kernel density estimator is:

$$\widehat{f}_h(x) = \frac{1}{nh}\sum_{i=1}^{n} K\left(\frac{x - x_i}{h}\right) \tag{3}$$

Table 1
Descriptive statistics include those that summarize the central tendency, disper-sion and shape of a dataset's distribution.

	mean	std	min	25 %	50 %	75 %	max
age	10.875	3.095	7	8	10	13.25	17
height [cm]	148.25	14.229	126	136.5	149	157.5	173
weight [Kg]	48.687	18.281	31	38	40.5	52.25	84
BMI [*Kg/cm2*]	21.062	4.202	16	18.75	20	22.5	28
IAP 0 % [mmHg]	0	0	0	0	0	0	0
IAP 35 % [mmHg]	4.309	0.331	3.85	4.2	4.2	4.287	4.9
IAP 50 % [mmHg]	6.812	0.655	6	6	7	7	8
IAP 75 % [mmHg]	9.234	0.709	8.25	9	9	9.187	10.5
IAP 100 % [mmHg]	12.312	0.946	11	12	12	12.25	14
Thorax circumference [cm]	77	10.757	63	70.5	74.5	82	97
Waist circumference 0 % [cm]	70.5	10.85	59	62.75	68	73.25	92
Waist circumference 50 % [cm]	77	14.869	63	64.875	70.75	82.5	107
Waist circumference 100 % [cm]	80.375	15.084	65	70	74	85.5	111
Hips circumferenc 0 % [cm]	80.656	13.501	67	72.625	75.5	84.25	105
Hips circumferenc 50 % [cm]	86.3125	17.954	69	74.25	78.5	90.75	125
Hips circumferenc 100 % [cm]	89.218	19.381	70	76.625	81	93.75	133
Antero-posterior diamete 0 % [cm]	15.781	2.065	11	15.375	16.5	17	18
Antero-posterior diamete 50 % [cm]	18.362	2.357	14	17.375	18	20.05	22.5
Antero-posterior diamete 100 % [cm]	21.25	2.581	17.5	19.5	21.75	23.5	26
Jugular notch/xiphoid length [cm]	14.218	2.032	11	13	13.75	16	17
Xifo-Bisiliac length 0 % [cm]	19.418	2.806	15.5	17.375	18.25	22	25
Xifo-Bisiliac length 50 % [cm]	24.175	3.502	20	21	23.75	26.25	32
Xifo-Bisiliac length 100 % [cm]	28.906	4.737	23	26	28	31	40
Midpoint bispinoiliac line / pubic symphysis length 0 % [cm]	6.925	1.078	5	6.375	7	7.625	9
Midpoint bispinoiliac line / pubic symphysis length 50 % [cm]	8.05	1.471	6	7	7.75	8.2	11.5
Midpoint bispinoiliac line / pubic symphysis length 100 % [cm]	7.837	0.805	7	7	7.5	8.5	9.5
Bis-spino-iliac length 0 % [cm]	23.281	3.188	17	21.625	23.5	24.625	29
Bis-spino-iliac length 50 % [cm]	25.968	3.844	19	23.5	25.5	30	31
Bis-spino-iliac length 100 % [cm]	29.043	4.696	21	26.25	29	32.25	36
Lateral abdominal wall thickness [cm]	33.218	18.007	13.7	18.967	30.715	44.4	67
Medial abdominal wall thickness [cm]	37.500	19.883	18.95	23.94	29.655	57.95	67.5
Rectus of the abdomen m. (under the navel) thickness [cm]	9.947	3.026	5.92	8.065	9.13	12.375	15
Rectus of the abdomen m. (over the navel) thickness [cm]	10.41	3.863	6.05	8.3	8.65	13.687	17
Lateral fat layer thickness [cm]	13.978	11.248	5.6	6.85	10.35	15.85	39
Oblique and Transverse m. (under the navel) thickness [cm]	19.625	9.436	8.88	12.147	18.18	29.102	33.76
Oblique and Transverse m. (over the navel) thickness [cm]	19.24	8.166	7.2	12.792	20.215	26.35	31
Medial fat layer thickness [cm]	27.090	16.393	9.2	16.817	21.465	43.14	52.5
Abdominal Volume 0 % [*cm3*]	23123.941	7657.868	12410.85	17344.182	21116.814	28851.929	36398.88
Abdominal Volume 50 % [*cm3*]	36644.577	11973.438	20045.76	28118.7	34,854	45413.82	63302.4
Abdominal Volume 100 % [*cm3*]	57071.344	19120.694	30002.7	43704.875	54795.355	67203.693	104499.2
Pelvic Volume 0 % [*cm3*]	1720.838	598.597	793.635	1311.456	1636.631	2020.655	3150.99
Pelvic Volume 50 % [*cm3*]	2510.310	1089.062	1171.350	1687.811	2303.320	2837.817	4858.299
Pelvic Volume 100 % [*cm3*]	2926.829	917.620	1391.150	2115.918	2985.804	3700.620	4266.932
Volume 0 % [*cm3*]	24844.779	8178.212	13204.485	18737.148	23156.113	30855.032	39417.99
Volume 35 % [*cm3*]	31618.676	9461.438	17605.98	25793.048	29050.625	39336.153	50158.144
Volume 50 % [*cm3*]	39154.887	12616.618	21217.110	30217.009	36997.638	47972.592	66959.813
Volume 75 % [*cm3*]	48265.157	16574.951	24990.115	35969.767	45231.607	57254.765	87501.071
Volume 100 % [*cm3*]	63999.667	20113.540	34421.595	51889.371	58837.270	79736.616	106377.803

parameter called the bandwidth. Typically, h is chosen as small as the data will allow; however, there is always a trade-off between the bias of the estima-tor and its variance. Referring to Fig. 2(b), the KDE of ages by gender is unbalanced. Indeed, samples of male patients are mostly in the range [6,10] years old, while samples of female patients are mostly in the range [10,15] years old. The estimation of age's probability density highlights, instead, a bimodal distribution.

Various BMI are also covered within the dataset, as shown in Fig. 3 (a), highlighting a larger presence of samples with BMI 20 *kg/cm*2(4 samples).

Referring to Fig. 3(b), the KDE of BMI by gender is however balanced within the range [15,24] *kg/cm*2and shows higher indexes for males.

In terms of physical characteristics of patients, the dataset includes sam-ples that cover the weight in the range [30, 80] *kg*, except the range (45, 73] *kg*, and the height in the range [130, 170] *cm*. The values are well distributed among male and female samples, as shown in Fig. 4(a). Moreover, both weight and height have a Gaussian distribution, as shown respectively in Fig. 4(b) and 4(c). However, the KDE applied to the latter indicates the presence of a bimodal distribution, due to the missing value in the range (45, 73] *kg*.

4.2. Feature selection

An essential step in any data analysis is to select the most predictive variables. Feature selection [33] is, indeed, a technique employed for reducing the number of input variables by eliminating redundant or irrelevant features. Thus, the objective of such a methodology is identifying the most helpful group of features that can be used to build a useful model of the phenomena we studied. In other words, it makes the prediction process more accurate, because it i) decreases the over-

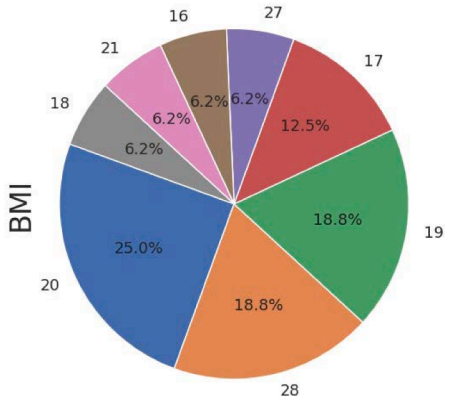

(a) Amount of BMI values.

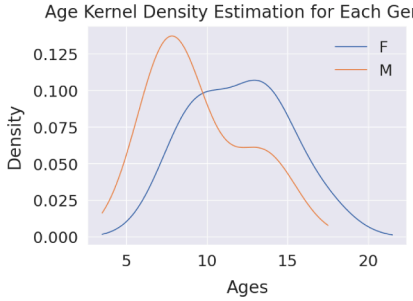

(b) Multivariate KDE relationship between gender and BMI.

Fig. 2. Study of the sample's balance by BMI.

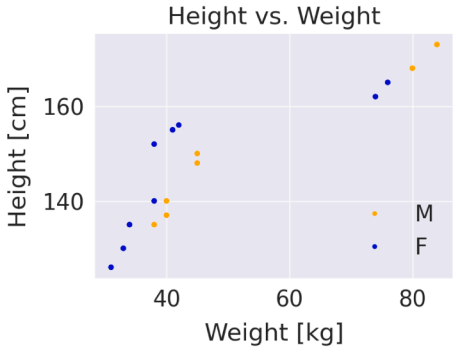

(a) Multivariate relationship between height, weight, and gender

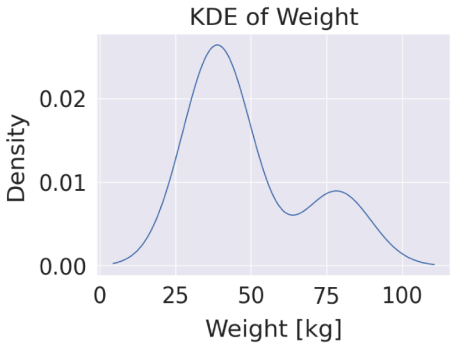

(b) Density distribution of weight

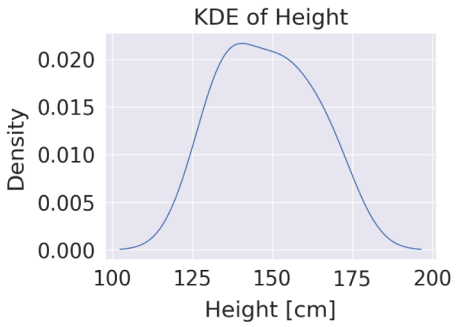

(c) Density distribution of height

Fig. 3. Study of samples balance by the couple weight-height.

fitting, ii) reduces the training time, and iii) creates more interpretable machine learning models. All of this turns into mitigating the bias.

Feature selection algorithms are categorized as either supervised (i.e., la-beled data) or unsupervised (i.e., unlabeled data). The latter is the kind of data we have in the dataset described in the section 3. Among the unsu-pervised techniques, methodologies are grouped as filter methods, wrapper methods, and embedded methods. While both the wrapper and embedded methods are applied along with a machine learning algorithms used to model the phenomena, the filter methods represent a selection of features based on statistics. In this regard, filter methods are appliable both on univariate or multivariate studies, in which, respectively, an ordered ranking list of features is established to inform the final selection of feature subset and the relevance of features is evaluated as a whole. In the following, we applied two filter methods, such as the variance thresholding and the correlation coefficient, to filter out features of the laparoscopy dataset, in order to prepare it for an unsupervised learning model (i.e., clusterization).

Before to follow up with the above-mentioned steps, the dataset needs to be normalized, which is the process of adjusting values measured on different scales to a notionally common scale. One of the most common ways to nor-malize data is applying the Min-Max-Normalization [34]. For every feature, the minimum value of that feature gets transformed into a 0, the maximum value gets transformed into a 1, and every other value gets transformed into a decimal between 0 and 1. The Min-Max Normalization applies the equation

$$x = \frac{value - \min}{\max - \min} \tag{4}$$

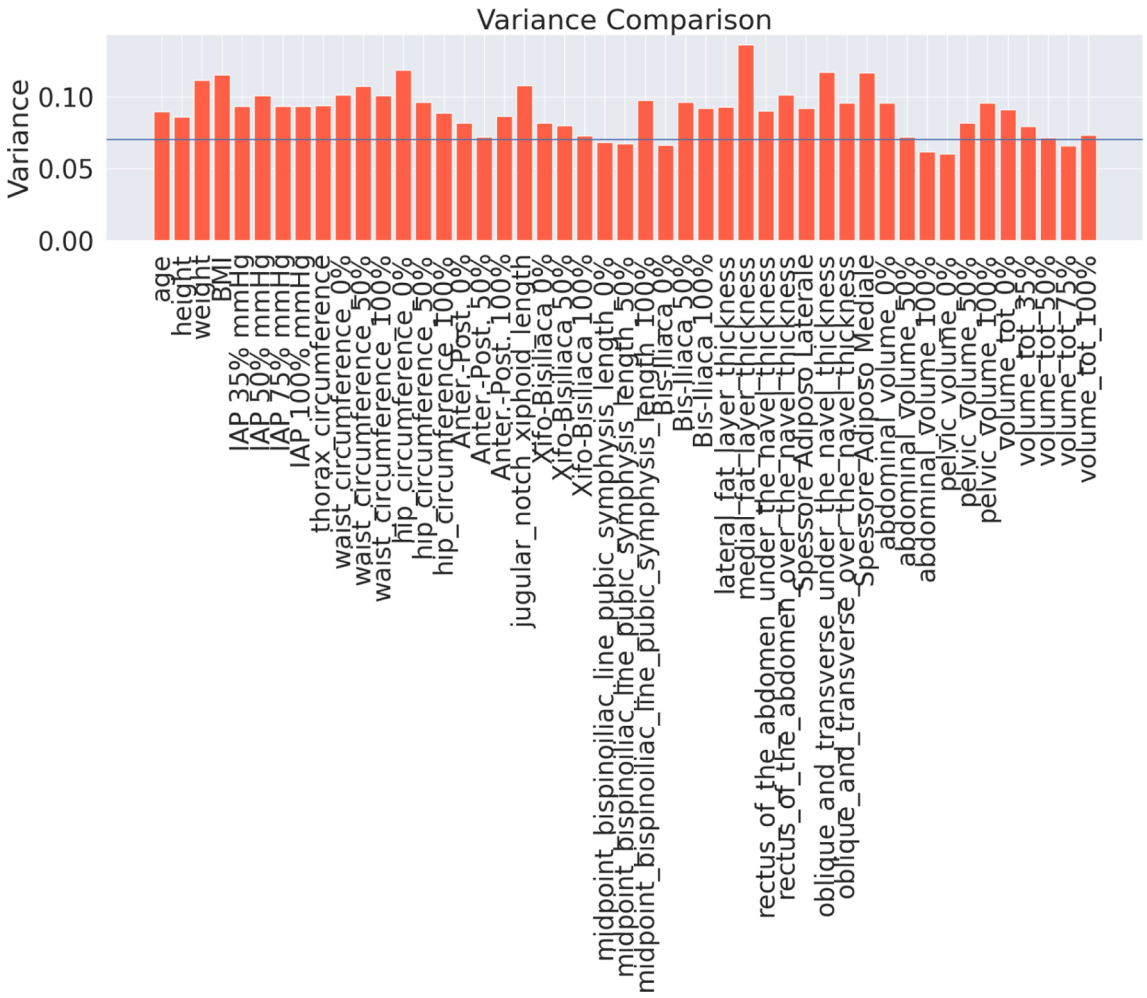

Fig. 4. VarianceThreshold (threshold = 0.07).

4.2.1. *Variance thresholding*

The Variance Thresholding [35] is a lightweight method of eliminating features with very low variance, i.e., features with not much useful informa-tion. Based on variance, it shows the variability in a distribution in a single metric. Moreover, it measures both how spread out the distribution is and the average squared distance from the mean, as expressed by the equation (5):

$$\sigma^2 = \frac{1}{n}\sum_{i=1}^{n}(x_i - \bar{x})^2 \tag{5}$$

Distributions with large values produce a large variance because each difference is squared. However, we are interested in studying if the distri-bution contains useful information. In this regard, we drop any feature or distribution with a variance close to 0.

According to [36,37], the Fig. 4 shows the output obtained when the Variance Thresholding method is applied to the laparoscopy dataset with a threshold of 0.07, which is a near-zero variance. Six features were removed and the remaining are later studies in terms of relationship between features. Indeed, this technique does not take into account the relationship between features or the connection between features and target.

4.2.2. *Correlation coefficient*

The correlation coefficient is a specific measure used to quantify the linear relationship between two variables. When using two variables, the formula compares the distance of each data point from the mean of the variable, defining how close the relationship between the two variables would lie to an imaginary line drawn between these data. This is why correlations identify.

linear relationships. However, correlations only consider the variables indi-cated and are unable to provide any further information on relationships that are external to the bivariate data. Furthermore, this type of analysis cannot detect data outliers, nor correctly identify curvilinear relationships.

The correlation coefficient r is a value with no unit of measurement and defined between −1 and 1. Statistical significance is indicated by means of a p-value. Therefore, correlations are usually written using two fundamental numbers: r and p. Regarding the meaning of r, the closer this is to zero, the weaker the linear correlation is. A positive r-value indicates a positive correlation, in which the values of the two variables tend to increase in par-.

allel. A negative r-value, on the other hand, indicates a negative correlation, in which the value of one variable tends to increase as the other decreases. The values 1 and −1 represent the"perfect" correlations, one positive and the other negative. Two perfectly correlated variables mutate together at a fixed rate. In this case, they have a linear relationship because, when placed in a scatter chart, all the data points can be connected to each other via a straight line. The p-value is used to determine whether, on the basis of what is observed on the sample, it can be significantly concluded that the correlation coefficient of the population is different from zero.

Pearson's correlation coefficient r is the best known statistical technique for evaluating the linear correlation between two variables,

but it involves the verification of some controls: (i) the two variables must both be quantitative, (ii) the two quantitative variables must be paired on the same cases, (iii) the correlation graph must show a linear relationship between the two variables, (iv) they must not be influenced by outliers, and (v) the distribution of both variables must be normal. The conditions (i) and (ii) are verified by dataset design. The condition (iii) is verified a posteriori. The condition (iv) is, instead, verified by the collection protocol. The conditions (v) is verified by applying the Shapiro-Wilk test [38], which is a test of normality, it determines whether the given sample comes from the normal distribution or not. Indeed, the Shapiro-Wilk test is one of the most powerful tests It is a test for the for verifying normality, especially for small samples.

verification of statistical hypotheses. It was introduced in 1965 by Samuel Shapiro and Martin Wilk. The verification of normality occurs by comparing two alternative estimators of the variance $\sigma 2$: (i) a non-parametric estimator based on the optimal linear combination of the order statistic of a random variable normal to the numerator; and (ii) the usual parametric estimator,

i.e., the sample variance, in the denominator.

$$W = \frac{\left(\sum_{i=1}^{n} a_i x_i\right)^2}{\sum_{i=1}^{n} (x_i - \bar{x})^2} \tag{6}$$

where xi is the i-th smallest value (rank i) of the sample; $\bar{x} = (x1 + \cdots + xn)/n$ is the arithmetic mean of the sample; and the constants ai are given by

$$(a_1, \ldots, a_n) = \frac{m^{\top} V^{-1}}{\left(m^{\top} V^{-1} V^{-1} m\right)^{1/2}} \tag{7}$$

where $m = (m1, \ldots, mn)\top$and $m1, \ldots, mn$ are the expected values of the ranks of a standardized random number, and V is the matrix of the.

covariance of these ranks. The W statistic can take values from 0 to 1. If the value of the W statistic is too small, the test rejects the null hypothesis that the sample values are distributed as a normal random variable. The weights for the linear combination are available in appropriate tables. The W statistic can be interpreted as the square of the correlation coefficient in a quantile–quantile diagram. The result of applying the Shapiro-Wilk test to the laparoscopy dataset, previously filtered with the Variance Threasholding method, is shown in the Fig. 5. The p-value threshold under which features were dropped out is set to 0.05, as suggested in [39].

The remaining 26 features were then studied with the Pearson's corre-.

lation coefficient. Features with a correlation higher than 95 % with other features bring low information to the model. These features are, therefore, dropped out. The resulting matrix correlation is then shown in the Fig. 6. (Fig. 7.).

Among the remaining features, both the thorax and xifo-bisialic distri-butions, for example, are strongly correlated with the abdomen volumes. At the same way, xifo-bisialic and bisialic are both correlated with the pelvis volumes. To verify the condition (iii) of the Pearson's correlation coefficient above-mentioned, the Fig. 8(a) and 8(b) are

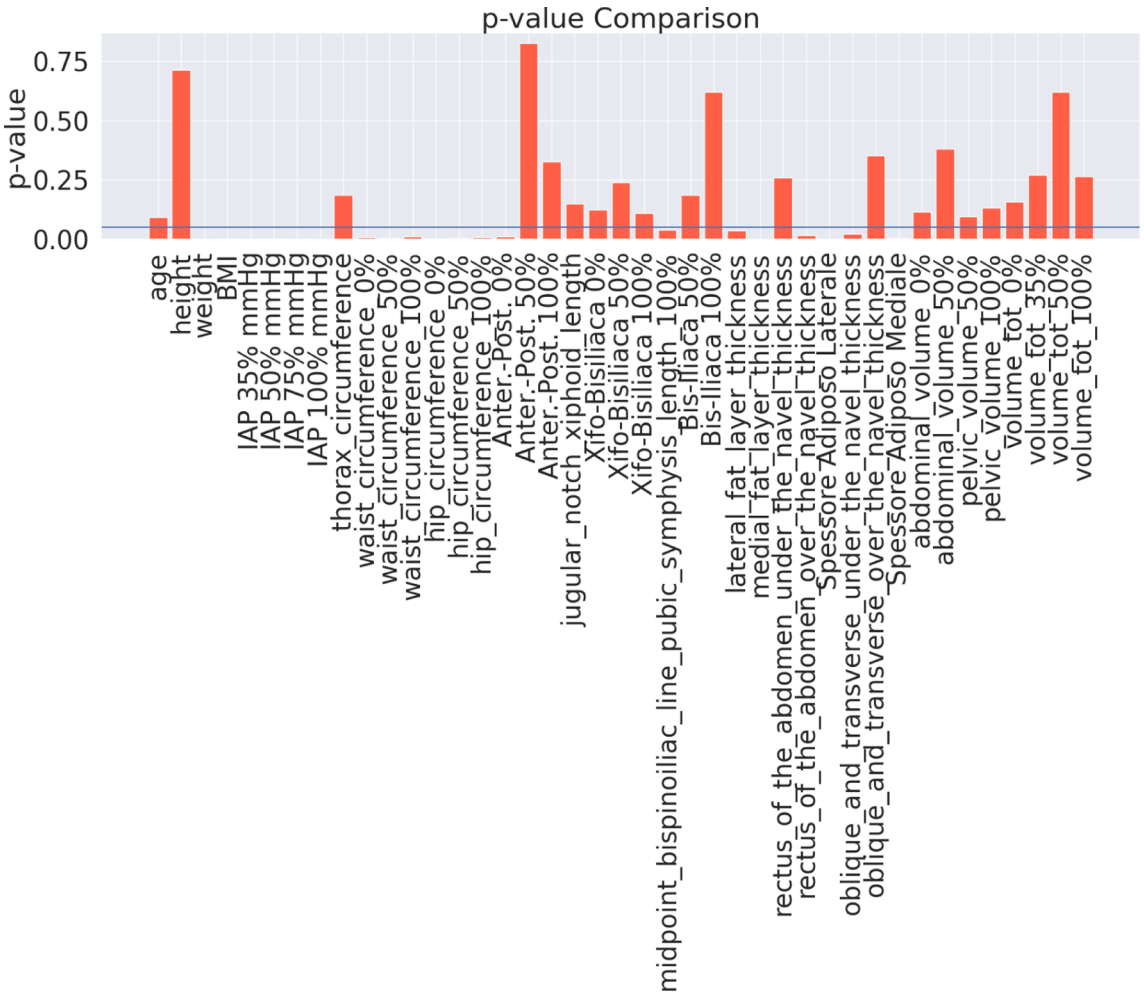

Fig. 5. p-values (threshold = 0.05).

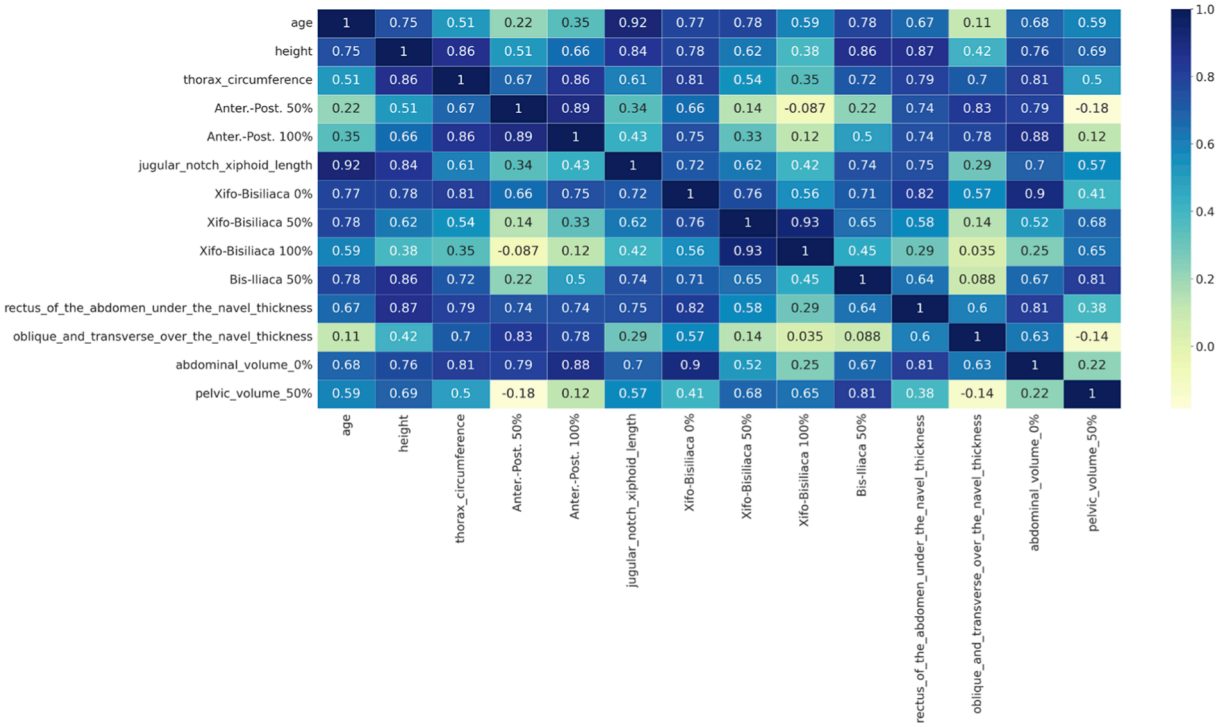

Fig. 6. Pearson correlation.

reported for studying the linear correlation. According to that figures, all curves are overlapped, and the condition is, therefore, verified.

5. Discussion

The clinical relevance of this study is crucial since we aim to reach def-inite pressure for each individual, creating the best working space without risk linked to the excess intra-abdominal pressure. This is particularly im-portant in young infants, below 10Kg, in which the effect of high pressure.

could negatively affect both the pulmonary expansion and the venous re-turn. Furthermore, increasing the intra-abdominal pressure does not always increase the intra-abdominal volume due to the sigmoid nature of the ab-dominal compliance. In this regard, the relationship between pressure and volume is strongly influenced by the morphological characteristics of the pa-.

tient. Indeed, according to the methodology applied in the Section 4, we determined the features that best could fit a clustering process. For exam-ple, thorax circumference and xifo-bisiliac length are both strongly correlated with volumes when insufflated with the 35 %, 50 % and 100 % of $CO2$. How-ever, the optimum number of clusters is no often obvious. Fortunately, there is a way of determining this mathematically.

Let's graph the relationship between the number of clusters and Within Cluster Sum of Squares (WCSS). Therefore, let's select the number of clusters where the change in *WCSS* begins to level off (Elbow method [40]). in this regard, WCSS is defined as the sum of the squared distance between each member of the cluster and its centroid, just as follows:

$$WCSS = \sum_{i=1}^{m} (x_i - c_i)^2 \tag{8}$$

To determine the best cluster numbers by using the Elbow method, we train multiple KMeans Clustering models [41] using a different number of clusters and storing the value of the inertia property (*WCSS*) every time. When the WCSS are plotted and the plot looks like an arm, then the"elbow", which is the point of inflection on the curve, is the best umber of the cluster. The Fig. 5 shows the result of the Elbow method, along with the time needed to train the clustering model for different K values included in the range [2,10]. The resulting optimal k value is 5.

6. Conclusion

This is the first preliminary attempt to standardize a laparoscopy surgery protocol in precision medicine by using a predictive approach. More specifi-cally, we theorized the possibility to create multiple clusters of pediatric in-dividuals, according to clinical characteristics and morphological conditions. Therefore, studying the abdominal compliance, which is the relation between the IAP and the IAV, as a multiple set of curves that will tailor the amount of $CO2$ insufflated to individuals.

In this regard, we firstly proposed a data acquisition protocol that approx-imates the thorax section as a cylinder and the pelvis section as a half-sphere. We studied the data model in terms of descriptive univariate and multivariate analysis, as well as the best predictors that fit a clustering process. Feature selection has been carried on by applying filter methods, such as the variance.

thresholding and the Pearson's correlation. Data analysis proved that there are strong correlations among features referring to thorax circumference and xifo-bisialic lenght with the sum of thorax and pelvis volumes. This leads to identify the optimal number of clusters through the Elbow method, which is set to 5.

We planned to extend that work with appropriate technical means. In terms of dataset, we aim to (i) include samples that cover pediatric patients under 7 years old, (ii) normalize the age distribution for each gender to fit a Gaussian distribution, and (iii) include patients with a weight within the range (45, 73] *kg*. Dataset must be enlarged to obtain accurate results and build relevant clusters. Given that this work is the first stage of longer research, we plan further activities as follows: (i) we aim to study the ab-dominal compliance of the presented dataset, proposing innovative (e.g., by using biological inspired artificial intelligence) methodologies that will help in fitting the P-V curve (e.g., a sigmoid) outperforming the state of the art.

[42]. Furthermore, (ii) we plan to apply different unsupervised

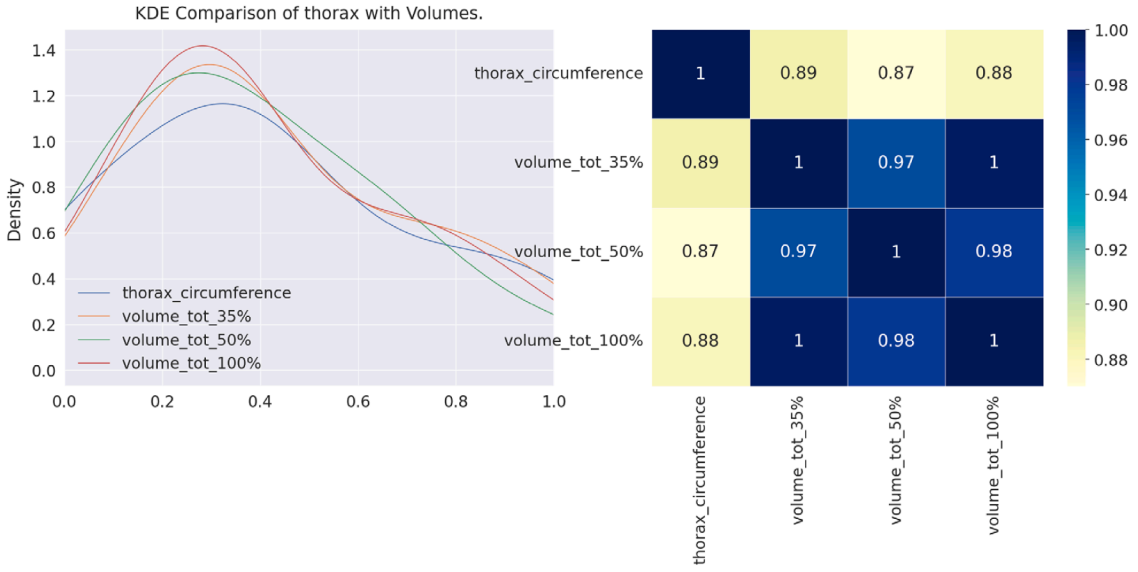

(a) Comparison of distribution between thorax circumference and volumes

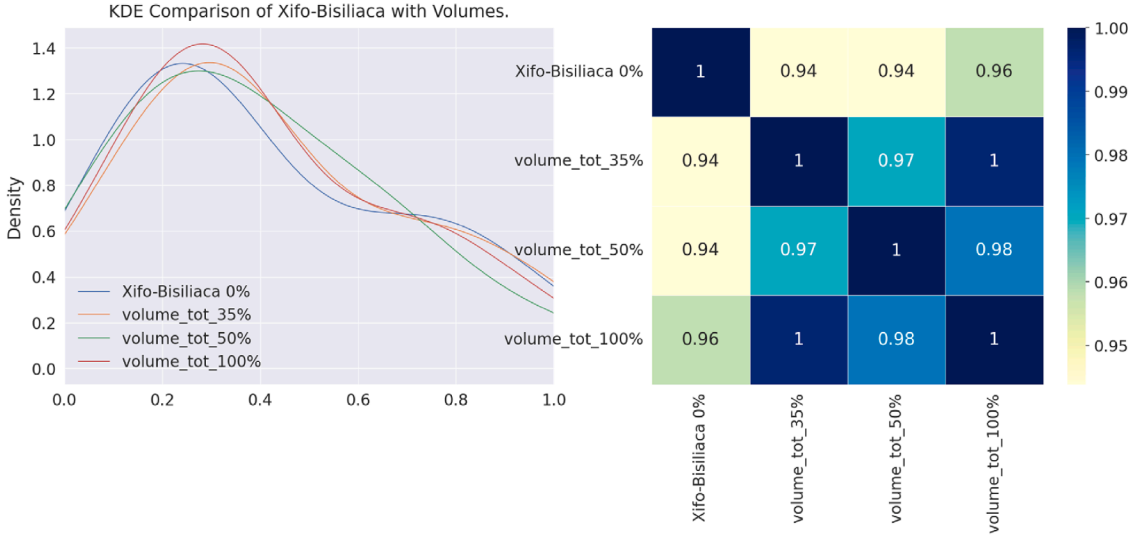

(b) Comparison of distribution between Xifo-Bisiliac length and volumes

Fig. 7. Comparison of features distribution with the volume.

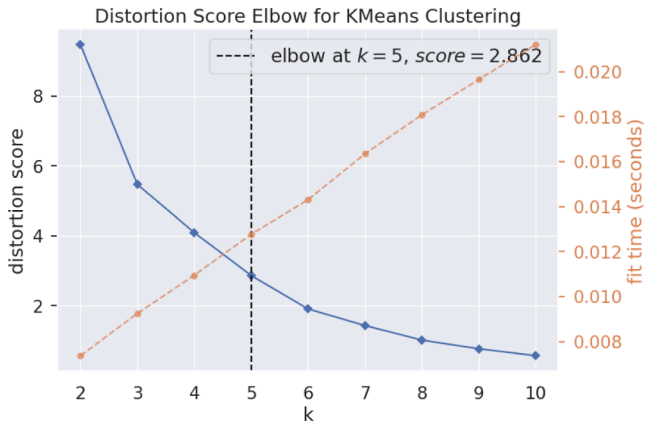

Fig. 8. The result of the Elbow method highlights that the optimal number of cluster is 5.

methods for identifying the best clustering process that will lead to create a set of P-V curves. Moreover, (iii) we want to use those clusters for providing to physi-cians a real-time tool usable during the laparoscopy surgery, integrating the methodology within a smart application.

Declaration of Competing Interest

The authors declare that they have no known competing financial interests or personal relationships that could have appeared to influence the work reported in this paper.

Data availability

The data that has been used is confidential.

Acknowledgement

This work was supported by the Italian PON “Ricerca e Innovazione”2014-2020 - “Machine Learning Advanced Algorithms and

Solutions for eHealth scenarios" (CUP J45F21001750007).

References

[1] F.S. Collins, H. Varmus, A new initiative on precision medicine, N. Engl. J. Med. 372 (2015) 793–795, https://doi.org/10.1056/NEJMP1500523.

[2] A.-M. Koivusalo, L. Lindgren, Respiratory mechanics during laparo- scopic cholecystectomy, Anesthesia Analgesia 89 (1999).

[3] J. Neudecker, S. Sauerland, E. Neugebauer, R. Bergamaschi, H.J. Bonjer, A. Cuschieri, K.-H. Fuchs, C. Jacobi, F.W. Jansen, A.-M. Koivusalo, A. Lacy, M. J. McMahon, B. Millat, W. Schwenk, The eu-ropean association for endoscopic surgery clinical practice guideline on the pneumoperitoneum for laparoscopic surgery, Surg. Endosc. 16 (2002) 1121–1143, https://doi.org/10.1007/s00464-001-9166-7.

[4] D.E. Ott, Abdominal Compliance and Laparoscopy: A Review (2019), https://doi.org/10.4293/JSLS.2018.00080.

[5] I. Dagogo-Jack, A.T. Shaw, Tumour heterogeneity and resistance to cancer therapies, Nat. Rev. Clinical Oncology 15 (2018) 81–94, https://doi.org/10.1038/nrclinonc.2017.166.

[6] U. Sahin, E. Derhovanessian, M. Miller, B.-P. Kloke, P. Simon, M.L. öwer, V. Bukur, A.D. Tadmor, U. Luxemburger, B. Schrörs, T. Omokoko, M. Vormehr, C. Albrecht, A. Paruzynski, A.N. Kuhn, J. Buck, S. Heesch, K.H. Schreeb, F. Müller, I. Ortseifer, I. Vogler, E. Godehardt, S. Attig, R. Rae, A. Breitkreuz, C. Tolliver, M. Suchan, G. Martic, A. Hohberger, P. Sorn, J. Diekmann, J. Ciesla, O. Waks-mann, A.-K. Brück, M. Witt, M. Zillgen, A. Rothermel, B. Kase-mann, D. Langer, S. Bolte, M. Diken, S. Kreiter, R. Nemecek, C. Gebhardt, S. Grabbe, C. Höller, J. Utikal, C. Huber, C. Loquai, Özlem Tureci Personalized rna mutanome vaccines mobilize poly-specific therapeutic immunity against cancer, Nature 547 (2017) 222–226, https://doi.org/10.1038/nature23003.

[7] Y. Harada, A. Sato, H. Nakamura, K. Kai, S. Kitamura, T. Nakamura, Y. Kurihara, S. Ikeda, E. Sueoka, S. Kimura, N. Sueoka-Aragane, Anti-cancer effect of afatinib, dual inhibitor of her2 and egfr, on novel mu-tation her2 e401g in models of patient-derived cancer, BMC Cancer 23 (2023) 77, https://doi.org/10.1186/s12885-022-10428-3.

[8] J. Xu, D. Xu, Q. Wei, Y. Zhou, Automatic classification of male and fe-male skeletal muscles using ultrasound imaging, Biomedical Signal pro-Cessing and Control 57 (2020) 101731, https://doi.org/10.1016/J.BSPC.2019.101731.

[9] J. Yang, J. Tu, X. Zhang, S. Yu, X. Zheng, Tse deeplab: An efficient vi-sual transformer for medical image segmentation, Biomedical Signal pro-Cessing and Control 80 (2023) 104376, https://doi.org/10.1016/J.BSPC.2022.104376.

[10] U. Boggi, Precision surgery, Updates Surg. 75 (2023) 3–5, https://doi.org/10.1007/s13304-022-01447-7.

[11] V. W. Rusch, Initiating the era of "precision" lung cancer surgery, https://doi.org/10.1056/NEJMe2215647 388 2023 557 558 10.1056/NEJME2215647.

[12] J.M. Arbeit, Molecules, cancer, and the surgeon: A review of molecular biology and its implications for surgical oncology, Ann. Surg. 212 (1990).

[13] P. Tejedor F. Sagias J. S. Khan The use of enhanced technologies in robotic surgery and its impact on outcomes in rectal cancer: A system-atic review https://doi.org/10.1177/1553350620928277 27 2020 384 391 10.1177/1553350620928277.

[14] C.A. Molina, D.M. Sciubba, J.K. Greenberg, M. Khan, T. Witham, Clinical accuracy, technical precision, and workflow of the first in human use of an augmented-reality head-mounted display stereotactic naviga-tion system for spine surgery, Operative Neurosurgery 20 (2021) 300–309, https://doi.org/10.1093/ONS/OPAA398.

[15] Z. Li, K.C. Koban, T.L. Schenck, R.E. Giunta, Q. Li, Y. Sun, Artificial intelligence in dermatology image analysis: Current developments and future trends, J. Clin. Med. 11 (2022) 6826, https://doi.org/10.3390/JCM11226826.

[16] Y. Okagawa, S. Abe, M. Yamada, I. Oda, Y. Saito, Artificial intelligence in endoscopy, Dig. Dis. Sci. 67 (5) (2021) 1553–1572, https://doi.org/10.1007/S10620-021-07086-Z.

[17] S. Walz, V. Aslani, O. Sawodny, A. Stenzl, Robotic radical cystectomy -more precision needed? Curr. Opin. Urol. 33 (2023) 157–162, https://doi.org/10.1097/MOU.0000000000001072.

[18] L. Jehi Machine learning for precision epilepsy surgery, https://doi.org/10.1177/15357597221150055 (2023) 1535759722115 00doi:10.1177/15357597221150055.

[19] A.M.L. Santilli, K. Ren, R. Oleschuk, M. Kaufmann, J. Rudan, G. Fichtinger, P. Mousavi, Application of intraoperative mass spec- trometry and data analytics for oncological margin detection, a review, IEEE Trans. Biomed. Eng. 69 (2022) 2220–2232, https://doi.org/10.1109/TBME.2021.3139992.

[20] N. Ogrinc, P. Saudemont, Z. Takats, M. Salzet, I. Fournier, Cancer surgery 2.0: Guidance by real-time molecular tech- nologies, Trends Mol. Med. 27 (2021) 602–615, https://doi.org/10.1016/J.MOLMED.2021.04.001.

[21] D. Schlanger, F. Graur, C. Popa, E. Mois, N.A. Hajjar, The role of artificial intelligence in pancreatic surgery: A systematic review, Z/METRICS, Up-dates in Surgery 74 (2022) 417–429, https://doi.org/10.1007/S13304-022-01255-.

[22] J.P. Mulier, B. Dillemans, M. Crombach, C. Missant, A.T.H. Sels, On the abdominal pressure volume relationship, The Internet Journal of Anesthesiology 21 (2008) 5221–5231.

[23] G. Mazzinari, O. Diaz-Cambronero, A. Serpa Neto, A. Martínez, L. Rovira, M. Argente Navarro, M. Malbrain, P. Pelosi, M. Gama de Abreu, M. Hollmann, M. Schultz, for the IPPColLapSe study in-vestigators, Modeling intra-abdominal volume and respiratory driv-ing pressure during pneumoperitoneum insufflation-a patient-level data meta-analysis, J. Appl. Physiol. 130 (3) (2021) 721–728, https://doi.org/10.1152/japplphysiol.00814.2020.

[24] J. Vlot, R. Wijnen, R.J. Stolker, K. Bax, Optimizing working space in porcine laparoscopy: Ct measurement of the effects of intra-abdominal pressure, Surg. Endosc. 27 (2013) 1668–1673, https://doi.org/10.1007/s00464-012-2654-0.

[25] B.L.D. Keulenaer, J.J.D. Waele, B. Powell, M.L. Malbrain, What is normal intra-abdominal pressure and how is it affected by positioning, body mass and positive end-expiratory pressure? Inten-Sive Care Medicine 35 (2009) 969–976, https://doi.org/10.1007/S00134-009-1445-0/TABLES/4.

[26] M.L.N.G. Malbrain, D.J. Roberts, I.D. Laet, J.J.D. Waele, M. Sugrue, A. Schachtrupp, J. Duchesne, G.V. Ramshorst, B.D. Keule-naer, A.W. Kirkpatrick, S. Ahmadi-Noorbakhsh, J. Mulier, R. Ivatury, F. Pracca, R. Wise, P. Pelosi, The role of abdominal compliance, the neglected parameter in critically ill patients — A consensus review of 16. part 1: Definitions and pathophysiology, Anaesthesiology Intensive Therapy 46 (2019) 392–405, https://doi.org/10.5603/AIT.2014.0062.

[27] M.L.N.G. Malbrain, I.D. Laet, J.J.D. Waele, M. Sugrue, A. Schachtrupp, J. Duchesne, G.V. Ramshorst, B.D. Keulenaer, A.W. Kirkpatrick, S. Ahmadi-Noorbakhsh, J. Mulier, P. Pelosi, R. Ivatury, F. Pracca, M. David, D.J. Roberts, The role of abdominal compli-ance, the neglected parameter in critically ill patients — a consensus review of 16. part 2: Measurement techniques and management rec-ommendations, Anaesthesiology Intensive Therapy 46 (2019) 406–432, https://doi.org/10.5603/AIT.2014.0063.

[28] M.L. Malbrain, Y. Peeters, R. Wise, The neglected role of abdomi-nal compliance in organ-organ interactions, Crit. Care 20 (3) (2016), https://doi.org/10.1186/S13054-016-1220-X.

[29] A.W. Kirkpatrick, D.J. Roberts, J.D. Waele, R. Jaeschke, M.L. Malbrain, B. D. Keulenaer, J. Duchesne, M. Bjorck, A. Leppaniemi, J.C. Ejike, M. Sugrue, M. Cheatham, R. Ivatury, C.G. Ball, A.R. Blaser, A. Regli, Z.J. Balogh, S. D'Amours, D. Debergh, M. Ka-plan, E. Kimball, C. Olvera, Intra-abdominal hypertension and the ab-dominal compartment syndrome: Updated consensus definitions and clinical practice guidelines from the world society of the abdominal compartment syndrome, Intensive Care Med. 39 (2013) 1190–1206, https://doi.org/10.1007/S00134-013-2906-Z/TABLES/6.

[30] C. Song, A. Alijani, T. Frank, G. Hanna, A. Cuschieri, Elasticity of the living abdominal wall in laparoscopic surgery, J. Biomech. 39 (2006) 587–591, https://doi.org/10.1016/J.JBIOMECH.2004.12.019.

[31] R. Zhou, H. Cao, Q. Gao, Y. Guo, Q. Zhang, Z. Wang, L. Ma, X. Zhou, T. Tao, Y. Zhang, L. Li, H. Zhou, W. Cheng, Abdominal wall elasticity of children during pneumoperitoneum, Journal of Pediatric Surgery 55 (2020) 742–746, https://doi.org/10.1016/j.jpedsurg.2019.05.025.

[32] C. Becker, M.A. Plymale, J. Wennergren, C. Totten, K. Stigall, J.S. Roth, Compliance of the abdominal wall during laparoscopic insuffla-tion, Surg. Endosc. 31 (2017) 1947–1951, https://doi.org/10.1007/S00464-016-5201-6/METRICS.

[33] R. Kohavi, G.H. John, Wrappers for feature subset selec-tion, Artif. Intell. 97 (1) (1997) 273–324.

[34] A. Gumaei, M.M. Hassan, M.R. Hassan, A. Alelaiwi, G. Fortino, A hybrid feature extraction method with regularized extreme learning ma-chine for brain tumor classification, IEEE Access 7 (2019) 36266–36273, https://doi.org/10.1109/ACCESS.2019.2904145.

[35] Z. Hou, Q. Hu, W. Nowinski, On minimum variance thresh-olding, Pattern Recogn. Lett. 27 (14) (2006) 1732–1743, https://doi.org/10.1016/j.patrec.2006.04.012.

[36] M. Kuhn, K. Johnson, Applied predictive modeling, Springer New York (2013), https://doi.org/10.1007/978-1-4614-6849-3.

[37] M. Kuhn, Building predictive models in r using the caret package, Jour-Nal of Statistical Software 28 (5) (2008) 1–26, https://doi.org/10.18637/jss.v028.i05.

[38] S.S. Shapiro, M.B. Wilk, An analysis of variance test for normality (complete samples), Biometrika 52 (3/4) (1965) 591–611.

[39] J. Berkson, Tests of significance considered as evidence, J. Am. Stat. Assoc. 37 (219) (1942) 325–335, https://doi.org/10.1080/01621459.1942.10501760.

[40] M.A. Syakur, B.K. Khotimah, E.M.S. Rochman, B.D. Satoto, In-tegration k-means clustering method and elbow method for identifica-tion of the best customer profile cluster, IOP Conference Series: Ma-Terials Science and Engineering 336 (2018) 012017, https://doi.org/10.1088/1757-899x/336/1/012017.

[41] A. K. Jain Data clustering: 50 years beyond k-means Pattern Recog-nition Letters 31 (8) (2010) 651–666 award winning papers from the 19th International Conference on Pattern Recognition (ICPR) 10.1016/j.patrec.2009.09.011.

[42] J.G. Venegas, R.S. Harris, B.A. Simon, A com-prehensive equation for the pulmonary pressure-volume curve, J. Appl. Physiol. 84 (1998) 389–395, https://doi.org/10.1152/JAPPL.1998.84.1.389/ASSET/IMAGES/LARGE/JAPP0515407.JPEG.